Divergence of catalytic systems in the zinc-catalysed alkylation of benzaldehyde mediated by chiral proline-based ligands

Thibault Thierry, Yannick Geiger, Stéphane Bellemin-Laponnaz

Divergence of catalytic systems in the zinc-catalysed alkylation of benzaldehyde mediated by chiral proline-based ligands.

Thibault Thierry,[1]+ Yannick Geiger,[1,2]+ and Stéphane Bellemin-Laponnaz*[1]

[1] Dr T. Thierry, Dr Y. Geiger, Dr S. Bellemin-Laponnaz
Institut de Physique et Chimie des Matériaux de Strasbourg, Université de Strasbourg-CNRS UMR 7504,
23 rue du Loess, BP 43, Cedex 2,
67034 Strasbourg, France
E-mail: bellemin@unistra.fr

[2] Current address:
Institut de Science et d'Ingénierie Supramoléculaires, Université de Strasbourg-CNRS UMR 7006
8 allée Gaspard Monge, BP 70028 Cedex,
67083 Strasbourg, France

[+] These authors contributed equally to this work.

Orcid number: 0000-0003-0342-2391 (T.T.), 0000-0003-2280-7107 (Y.G.), 0000-0001-9462-5703 (SBL).

Abstract

Asymmetric catalysis has expanded the range of chiral products readily accessible through increasingly efficient synthetic catalysts. The development of these catalysts often starts with a result obtained by systematic screening of known privileged chiral structures and assumes that the active species would be an isolated monomolecular species. Here, we report the study of three proline-derived ligands, diphenyl-N-methyl-prolinol, diphenylprolinol and 5-(hydroxydiphenylmethyl)-2-pyrrolidinone in the zinc-catalysed alkylation of benzaldehyde. The three ligands exhibit different system-level behaviour, characterised by multiple levels of aggregation that may be catalytically active simultaneously. While diphenyl-N-methyl-prolinol behaves as expected from a mechanistic point of view, diphenylprolinol shows enantiodivergence during the reaction due to an asymmetric autoinduction process. With 5-(hydroxydiphenylmethyl)-2-pyrrolidinone, we were able to establish the possibility of at least trimeric active species in equilibrium with less aggregated active species. Simulations using a mathematical model confirm the possibility of such systems-level behaviour. Parallel study of the three systems reveals three distinct system-level behaviours that are central to the efficiency of the catalytic reaction.

Main Text

The design of chiral catalysts is a challenging task and the complexity of many catalytic processes precludes a purely rational approach based on mechanistic and structural criteria. Therefore, most new chiral catalysts are still discovered with an element of empiricism, intuition and especially by taking advantage of previous knowledge of specific molecular structures.[1–3] The methodology that aims at achieving high catalytic activity and enantioselectivity is usually based on the use of scaffolds of natural chiral products and generally relies on the assumption that the active species would be a monomeric species.

However, aggregation of the catalyst -or the catalyst itself being an aggregate- can lead to more complex behaviour than expected, especially in organometallic catalysis, but not only.[4,5] It can affect the overall reaction kinetics and the overall enantiomeric excess of the product. Such systems-level behaviour in asymmetric catalysis was first investigated by Kagan, who found that a non-linear relationship between the product ee (ee_P) and the ligand ee (ee_L) ("non-linear effect", NLE) is indicative of catalyst aggregation.[6,7] Kagan's rationalization of the concepts by proposing different mathematically supported models opened the way to a better understanding of asymmetric catalytic mechanisms.[8–10] Since then, studies of nonlinear effects have become commonplace as the presence of NLEs is generally considered to be a fingerprint of catalyst aggregation or catalysis by multiligand complexes, with only few exceptions known in multi-step reactions.[11,12] Such study is therefore expected to provide an understanding of the catalytic system as a whole. However, asymmetric catalysis still contains black-box aspects and the conceptualization of mechanisms is always based on the assumption of a single active species. This is also the case for non-linear effect models, which consider only a single level of aggregation as the active species instead of multiple levels.

Recently we have established the importance of catalyst loading-dependent ee_P screening as a probe for multiple aggregation levels that are catalytically active at the same time.[13–17] This has led to an understanding of more complex NLEs, such as hyperpositive and enantiodivergent NLEs, which include a coexistence of active monomeric and active dimeric species. A higher degree of complexity seems attainable if one considers that higher levels of aggregation could be envisaged, such as a monomer-dimer-trimer system level as displayed in Fig. 1.

In this study, we show how three different ligands, issued from the same privileged chiral structure,[1] exhibit completely different systems-level behaviours and thus also different reaction outcomes. Mechanistic studies show that metal complexes aggregate and generate additional catalytic species in different ways - including an enantiodivergent system via an asymmetric autoinduction process, and a case where at least trimeric species are catalytically active.

Results and Discussion

Chiral ligands derived from proline are numerous and have demonstrated their usefulness in many enantioselective catalytic reactions, with or without metal.[18] Its scaffold (core structure) classifies this family as "privileged chiral catalysts", which prompted us to investigate whether these ligands show systems-level behaviour similar to their counterparts based on ephedrine[13–17] or camphor[19,20] in the zinc-catalysed alkylation of benzaldehyde. The reaction starts with the chiral aminoalcohol ligand reacting with a first equivalent of dialkylzinc, forming a ligand-alkylzinc complex that can activate benzaldehyde and another equivalent of dialkylzinc to give a chiral alkylzinc-alkoxide product.[21,22] The ligand-alkylzinc complex can also aggregate, giving rise to additional catalytic species in some cases.[13–17] We chose diphenyl-N-methyl-prolinol **DPMP (1)**, diphenylprolinol **DPP (2)** and 5-(hydroxydiphenylmethyl)-2-pyrrolidinone **DPPy (3)** as chiral ligands for our study, which are all derived from the

proline structure (Fig. 2).[21] All experiments described here were done in triplicates (except for kinetic monitoring) and demonstrated excellent reproducibility.

DPMP ligand (1)

Figure 3a displays the correlation between the enantiomeric excess of the product (ee_P) and the enantiomeric excess of the ligand (ee_L) for the asymmetric addition of diethylzinc to benzaldehyde in presence of **1**, an N-methylated prolinol ligand (the *S*-configuration is the major enantiomer in all our ligand studies) that was first introduced by Soai et al.[23,24] It exhibits a strongly positive nonlinear effect (i. e. datapoints are shifted away from the Ligand ee-axis compared to the dashed line; (+)-NLE) with a product of 93% ee in presence of the enantiopure ligand. We also performed a screening of the catalyst loading in presence of enantiopure ligand and this variation does not affect the enantioselectivity of the reaction (Fig. 3b); kinetic monitoring shows ee_P to stay also constant over time at several catalyst loadings (Fig. 3c). The study was completed by performing a temperature screening of the catalysis with the enantiopure ligand. A slight decrease of the product ee was observed while decreasing the temperature, as shown in Suppl. Fig. 1-2 in the Supporting Information.

With the scalemic ligand **1**, upon addition of diethylzinc, a white precipitate is observed while the enantiopure solutions remain clear.[25] Filtration and hydrolysis of one of these precipitates yielded the native ligand in its racemic form, suggesting the formation of heterochiral aggregates at the origin of the (+)-NLE. Altogether, the results suggest that only a single aggregation level has significant catalytic activity in this reaction. Additional studies by ^{1}H diffusion-ordered spectroscopy (DOSY) NMR experiments of enantiopure **1** reacted with $ZnEt_2$ in toluene-d_8 indicated of an aggregation level 1.9, suggesting that the complex exists almost exclusively as dimeric (**1**-ZnEt)$_2$ species (cf. Supplementary section I.4.1). Analysis of kinetic conversion profiles by VTNA[26–28] reveal a kinetic order of 0.5 in **1** (Suppl. Fig. 3), which is consistent with catalytically active monomers and a monomer-dimer equilibrium that is almost entirely shifted to the dimer;[26,29] catalytically active dimers would have an order between 1 and 2.[30] Thus, we are facing here a catalytic scheme identical to the case of the DAIB ligand described by Noyori: an active monomeric species in equilibrium with dimers that are inactive but induce NLEs by influencing the enantiomeric composition of the monomer (Fig. 3c).[19,20]

DPP ligand (2)

Ligand **2** is a non-methylated variant of **1** and shows a similar (+)-NLE with slightly decreased enantioselectivity (Fig. 4a, red line). Similar to **1**, a racemic precipitate formed during the NLE studies of **2**, which was reported to be a heterochiral dimer.[31,32] However, the screening of the catalyst loading with enantiopure **2** showed a very different picture (Fig. 4b): decreasing the catalyst loading from 20 to 0.25 mol% changed the reaction outcome from 82% ee (*S*)- to 19% ee (*R*)-product. A subsequent NLE study at 0.25 mol% catalyst loading gave only negative ee_P values with a close to linear ee_P/ee_L relationship (Fig. 4a, blue line). Increasing the temperature lead to an ee_P decrease at

several catalyst loadings (i. e. to *improved* enantioselectivity when ee_P is negative), causing at 2.5 mol% even a switch of the ee_P sign (Suppl. Fig. 5). ^{1}H DOSY NMR experiments of enantiopure **2**-ZnEt showed dimeric and monomeric zinc complexes, no higher aggregates were observed (cf. SI section I.4.2).

Although the (+)-NLE of ligand **2** in Fig. 4a suggests the system being similar to **1**, with a somewhat lower enantioselectivity and chiral amplification, the results in Fig. 3b show that this is misleading. The **2** system consists not of one but at least two non-racemic catalytic species yielding product of opposite signs. Taken together with the NMR data and the precedent of ephedrine-based ligands,[13–17] one could be tempted to conclude on a monomer-dimer system (cf. Fig. 1) with a monomeric **2**-ZnEt yielding the *(R)*-product which is in equilibrium with a dimeric complex yielding the opposite enantiomer. However, this would imply that monomeric **1**-ZnEt and **2**-ZnEt yield opposite enantiomer products, despite their almost identical structure. Furthermore, we found an unusual dependency of ee_P on conversion and catalyst loading with enantiopure **2** (Fig. 4c): at 20 mol%, ee_P remains constant at ca. 86% throughout the whole reaction, except for a slight drop in the last 20% conversion. But the lower the catalyst loading, the earlier and more pronounced the ee_P drop over time, with the ee_P at the start being roughly the same. This culminates in a spectacular breakdown from 72% to -20% ee_P at 0.25 mol% of **2**. Calculation of the reaction's enantioselectivity over specific time intervals shows that sharp drop happening already within the first 10% conversion, afterwards the enantioselectivity remains at -20 to -30% ee (Suppl. Figure 6c). If additional substrate and reagent are introduced at the end of the reaction, the cut-off value of -20% ee_P is then reached (at 2.5 mol% cat. loading) or maintained (0.25 mol%) (Suppl. Fig. 7). We also tested other aldehydes (i.e. para-cyano-benzaldehyde and para-trifluoromethyl-benzaldehyde) and the same behavior was observed in both cases (Suppl. Fig. 8). Comparable enantioselectivity changes over time were observed previously on a polymer-grafted[33] and a fused dimeric equivalent of **2.**[34]

Variation of ee_P over time was also observed with the *N*-benzyl ephedrine (NBE) ligand and $ZnMe_2$[13] but in a different manner: the observed ee_P increase remained limited (ca. 30% ee_P overall) and is similar for all studied catalyst loadings; only the ee_P at which the reaction starts was affected by the catalyst loading. This is consistent with the product associating with the catalyst as an inactive adduct (product inhibition), which decreases the concentration of available NBE-ZnMe and favours the more enantioselective monomer over the dimer, thus causing an ee_P increase over time (monomer-dimer model, Fig. 1). However, these observations are literally opposite to the present behaviour seen with **2** and $ZnEt_2$. We could exclude modification of **2**-ZnEt over time due to e. g. slow deprotonation of the NH-group (cf. comparison with an "aged" catalyst that was generated *in situ* 24h before adding the aldehyde substrate, Suppl. Fig. 9). Therefore, we had to consider also the possibility of asymmetric autoinduction, i. e. the association of catalyst and product to form a new catalytically active species with a different enantioselectivity (not to be mistaken with autocatalysis, where the product alone is catalytically active).[35–41] A classic way to probe for this is to add product before starting catalysis ("doping") and to compare the outcome with an undoped reaction. In our case this lead indeed to an ee_P decrease, the doping product being racemic or enantiopure *(S)* making no difference (cf. Suppl. Fig. 10). However, a product inhibition-induced shift in the mono-

/dimer equilibrium of an NBE-like monomer-dimer model might give a similar result. In order to discriminate between this and autoinduction, we conducted kinetic monitoring experiments under saturation conditions: high concentration (1.0 M benzaldehyde, 10 mol% **2**) was used so that the enantiopure **2**-ZnEt complex remained partially precipitated over the full duration of the reaction. Under these conditions, the concentrations of (**2**-ZnEt)$_2$ and **2**-ZnEt are fixed by the solubility and dimerization constants, respectively; on the other hand, a catalyst-product adduct can accumulate over time with increasing product concentration. In a product inhibition scenario ee_P would remain constant since it depends only on the monomer and dimer concentrations. However, we observed here a similar ee_P drop over time as in Figure 3c for 10 mol% **2** (Suppl. Fig. 11).

To further verify the autoinduction hypothesis, we built a mathematical model based on earlier work[15,16,25] (cf. also discussion below; the mathematical treatment can be found in the SI, section III.2) which includes monomeric and dimeric complexes (R, RR) as well as catalyst-product adducts of type RP_n (n = 1, 2, 3…). This allowed us to simulate enantioselectivity vs. conversion profiles at various catalyst loadings (Suppl. Fig. 12). With active dimers and RP (n = 1, Suppl. Fig. 12b) as adduct, we were able to qualitatively reproduce the decrease in enantioselectivity on conversion and the change in shape of the curve with decreasing catalyst loading. With RPP (n = 2, Suppl. Fig. 12c) the shape of the curve shape becomes sigmoidal and is even more similar to that in Figure 4c. Interestingly, catalytically active dimers are necessary for the model to generate any dependence on the catalyst loading; monomers can be also active, but they reduce the relative impact of the dimer (Suppl. Fig. 12d and 12e and following discussion). Overall, this further supports the autoinduction hypothesis presented in Figure 4c, even though it is unclear how the behaviour can span over such a low range of catalyst loading and why dimers would dominate over monomers in terms of catalytic activity, in stark contrast to the closely related ligand **1**. Literature data suggests that the aldehyde/$ZnEt_2$-ratio and the solvent seem to also have an important impact.[33,42]

DPPy ligand (3)

Ligand **3** is an oxygenated version of **2**, the secondary amine being changed into an amide group, and shows an even more complex behaviour than its two counterparts. With **3**, the NLE curve changes dramatically and displays enantiodivergence (Fig. 5a). The curve starts at 33% ee_P in the positive ee_P-range and falls down to quickly cross the ee_L-axis (at 80% ee_L) and ends up in the negative part of the ee_P-scale. In addition, a decrease of catalyst loading led to an ee_P increase with both enantiopure and 33% ee ligand (Fig. 5b). With enantiopure **3**, a bell-shaped curve was obtained in a temperature screening (Suppl. Fig. 14, yellow trace). It is interesting to note that the use of a 33% ee_L scalemic ligand gives the *(R)*-product whatever the temperature (Suppl. Fig. 14, blue trace). Monitoring ee_P over time at different catalyst loadings gave approximately parallel ee_P vs conversion profiles (Suppl. Fig. 15), close to what was observed with NBE,[13] which renders autoinduction as seen with ligand **2** unlikely. Ligand **3** exhibits the slowest conversion of all catalytic systems studied in this paper (Suppl. Fig. 16) and catalyst aging experiments showed no sign of slow NH deprotonation by excess $ZnEt_2$ (Suppl. Fig. 17).

The NLE in Fig. 5a could be, in principle, compatible with the monomer-dimer model. However, the strictly convex shape of the NLE is unusual: enantiodivergent NLEs of comparable magnitude calculated previously[15] are only partially convex and also cross the ee_L-axis at smaller values (an example is given in Fig. 7a below; cf. Suppl. Fig. 17 for visual examples of strictly and partially convex curves). Furthermore, the catalyst loading screening with enantiopure ligand (Fig. 5b, blue) should overlay with the right half (or more) of the observed NLE[13] (cf. also the plain blue lines in Figure 7a and b, below) but this is not the case here. The enantiopure catalyst loading screening suggests low ee_P-yielding aggregates and high-ee_P-yielding monomers/lower aggregates, but the sharp ee_P drop in Fig. 5a must originate from an additional catalytic aggregate that exists only with scalemic ligand and gives negative ee_P; the catalyst loading screening at 33% ee_L confirms this hypothesis (Fig. 5b, red). This implies that the system comprises three distinct non-*meso* (i. e. non-racemic) catalytic complexes, which is not possible in a monomer-dimer model in which there are only two (monomer and homochiral dimer). However, if the system's aggregation level is higher than 2, then additional catalytic species become available, including heterochiral aggregates (e. g. RRS and RSS in the case of trimers) that may cause a sharp ee_P drop as in Fig. 5a. ^{1}H DOSY NMR experiments of **3**-ZnEt at 33% ee_L (here, the enantiopure complex precipitates and complicates measurements whereas the scalemic complex does not) confirmed the system's tendency to higher-order aggregation: aggregates (presumably clusters or oligomers) with an average size of >2 nm were observed (curiously, the size increases with temperature, cf. SI section I.4.3), but trimeric species could also be identified in the mixture. The presence of an amide group is much likely to alter the coordination mode of ligand **3**, favouring higher-order aggregates. NLEs were reported on metallopolymers previously, which showed unusual bell-shaped curves but no enantiodivergence.[43,44]

To test the impact of higher than dimeric degrees of aggregation, we went on to the modelling of NLE- and ee_P vs cat. loading-curves. Previously, we transcribed the monomer-dimer competition model into a mathematical framework allowing the qualitative simulation of NLE curves.[15,16,25] We have extended this framework to trimers (Figure 6) and simulation of ee_P vs cat. loading-curves (the full mathematical treatment can be found in the SI, section III.3). The model now contains four different non-racemic species (monomers, homochiral dimers, homo- and heterochiral trimers) that can each yield a product with a distinct ee due to catalytic activity, in addition to the *meso*-dimer that can give racemic product. The framework is modular, i. e. some species can be considered as catalytically inactive by setting their respective kinetic constant to 0, or as inexistent by setting the respective equilibrium constant to 0. The model operates under steady state conditions (i. e. all equilibria are fast relative to the catalytic, product-forming steps), therefore the specific pathway for the formation of trimers, either directly from monomers or from dimers, is not relevant. Here, we chose the trimers to be directly in rapid equilibrium with the monomers, but we also investigated a dimer-trimer variant of the system without any monomeric species, where trimers necessarily depend on dimers (cf. SI section III.4). An excel spreadsheet using these models to simulate graphs is provided in the SI.

With the current model, we attempted to reproduce the key features of Figure 5 using three scenarios: a monomer-dimer (no trimers present, total of two non-*meso* catalysts), a monomer-trimer and a dimer-trimer system (no dimers resp. monomers present, total of three non-*meso* catalysts). Figure 7 shows some examples, with the data in Figure 5 in grey dots for comparison. We could not reproduce the main features of ligand **3** with the monomer-dimer system: with a first parameter set that gave an enantiodivergent NLE (Figure 6a, plain line), ee_P was found to decrease at lower catalyst loading instead of increasing, at both 100% (Figure 7b, plain blue line) and 33% ee_L (plain orange line). A second parameter set could reproduce the ee_P *vs* cat. loading at 100% ee_L (Figure 7b, dashed blue line) but failed to do so at 33% ee_L (dashed orange line) and the associated NLE is neither enantiodivergent nor hyperpositive (Figure 7a, dashed line). In contrast, with the monomer-trimer and dimer-trimer scenarios, we were able to produce enantiodivergent NLEs with a strictly convex shape close to that in Figure 5a (cf. Figures 7c and 7e, and Suppl. Fig. 17). Furthermore, ee_P increases with decreasing catalyst loading both at 100% and 33% ee_L (cf. Figures 7d and 7f), the latter crossing the x-axis, as in Figure 5b. As a control study, we applied additionally an ML1-2-3 system with inactive trimers (Suppl. Figure 19; contains two non-*meso* catalysts as in ML1-2). It resulted in a shift of the hyperpositive minimum compared to ML1-2 in Figure 7a+b, but the curve remained only partially convex. Altogether, only models comprising catalytically active trimers – and thus, implying three distinct non-*meso* catalysts – could qualitatively reproduce the data from ligand **3**. This supports the hypothesis of aggregates larger than dimers being catalytically active with ligand **3**.

Conclusion

In this study, we showed how different complex systems can emerge from a proline-based framework. The comparison between **1** and **2** is particularly striking: the removal of a methyl group on the nitrogen atom is sufficient to allow for a catalytically active catalyst-product adduct. Such asymmetric autoinduction was observed in diorganozinc additions before, but only in systems involving titanium complexes.[35,36] A possible explanation for that behaviour is the N-H in ligand **2** allowing for hydrogen bonding to the product zinc alkoxide, causing a change in ligand conformation. Ligand **3** exhibits even a completely different aggregation behaviour and is, to the best of our knowledge, the first example of a system with (at least) three non-racemic catalysts emerging from a single ligand. Even though a ligand structure might be well suited for single-species catalysis, its systems-level behaviour – which can have a heavy impact on reaction rates, yields and product ee – is often difficult to predict. Alkylzinc alkoxides are naturally prone to aggregation due to their Lewis acid/base bifunctionality and are thus an excellent field to study emerging systems-level behaviour.[45] This is particularly well illustrated by the recent mechanistic studies by the Denmark[46,47] and Trapp[48,49] groups on the autocatalytic Soai reaction,[50,51] which show small changes in functional groups lead to strongly altered structures and behaviours and possibly even to multiple autocatalytic pathways.[52] However, we expect such thing also in other catalytic reactions. For example, covalent organocatalysis often necessitates catalyst loadings of 10-20mol% (similar to the ones used in the present study)– aggregation effects might be well at play here, in addition to catalyst deactivation and side-reactions.[53–55]

Furthermore, the study shows how the combined analysis of NLEs and ee_P *vs* catalyst loading-plots, supported by kinetic studies, DOSY NMR and mathematical modelling, can give important insights into complex catalytic systems. This was achieved with almost no quantitative analysis: the interpretation of specific features (maxima/minima, curve convexity, enantiodivergence, rising or falling curves) in the graphs was sufficient and, in the case of ligand **1**, supported by the intuitive use of VTNA combined with some knowledge about kinetic orders in catalyst. We believe that these will further develop and become important tools in the analysis of complex catalytic systems.

Methods

General procedure for the catalytic tests

In a N_2-filled glovebox, chiral ligand **1**-**3** (20 mol%) and a magnetic stirring bar were placed in an oven-dried vial, which was then closed with a septum-containing screwcap. The vial was put out of the glovebox and a 1.5 M $ZnEt_2$ solution in toluene (1.2 equiv.; 400 µL; 600 µmol) was added via syringe; gas evolution occurred. After dry toluene addition (2.93 mL), the mixture was stirred for 10 min, then was set to the desired temperature and benzaldehyde (1 equiv.; 51 µL; 500 µmol) was added via syringe. The yellow solution stirred 6 hours at the same temperature and turned colorless, then was quenched carefully with 3 M aqueous HCl in an ice-water bath under vigorous stirring. The organic phase was isolated, dried over Na_2SO_4, then an aliquot was taken and analysed by chiral stationary phase GC without further purification.

Data availability

The data that support the findings of this study are available in the Supporting Information.

Acknowledgements

This research was supported by the Interdisciplinary Thematic Institute ITI-CSC via the IdEx Unistra (ANR-10-IDEX-0002) within the program Investissement d'Avenir (T. T.) and the Ministère de l'Enseignement Supérieur et de la Recherche (MESR) for a PhD grant to Y.G. We thank the NMR department CNRS FR2010 Strasbourg and particularly Bruno Vincent for his valuable studies. We also thank Thierry Achard, Aline Maisse-François and Emilie Couzigné from IPCMS Strasbourg.

Author Contributions

T.T. performed the synthetic experiments, Y. G. made the mathematical models and computed simulations. T.T., Y.G. and S.B.L. performed the data analyses. S.B.L. conceptualized and supervised the study, and wrote the manuscript with T.T. and Y.G.

Competing interests

The authors declare no competing interests.

Figure Legends/Captions

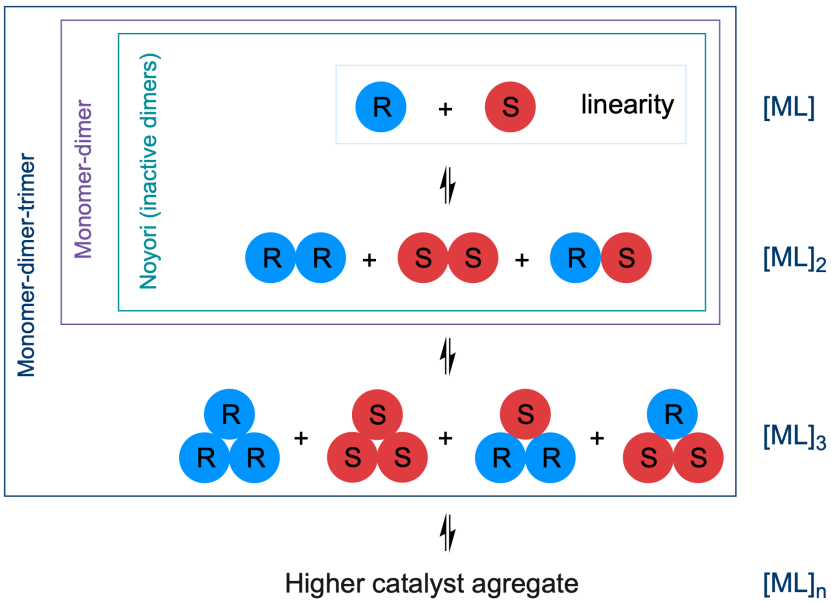

Figure 1. General figure for the systems-level behaviour in asymmetric catalysis. Each circle represents a mononuclear species of type [ML], M being the metal and L the ligand of R or S configuration. A system consisting of catalytically active monomeric complexes ([ML]) does not give rise to any non-linear effect, but systems composed of active dimers ($[ML]_2$) or trimers ($[ML]_3$) do. Catalytic systems can also bear several levels of aggregation at the same time, with all (monomer-dimer model) or only some of the species (Noyori model) being catalytically active. These typically (but not necessarily) give rise to NLEs and their curve can become more complex as the number of different species increases.

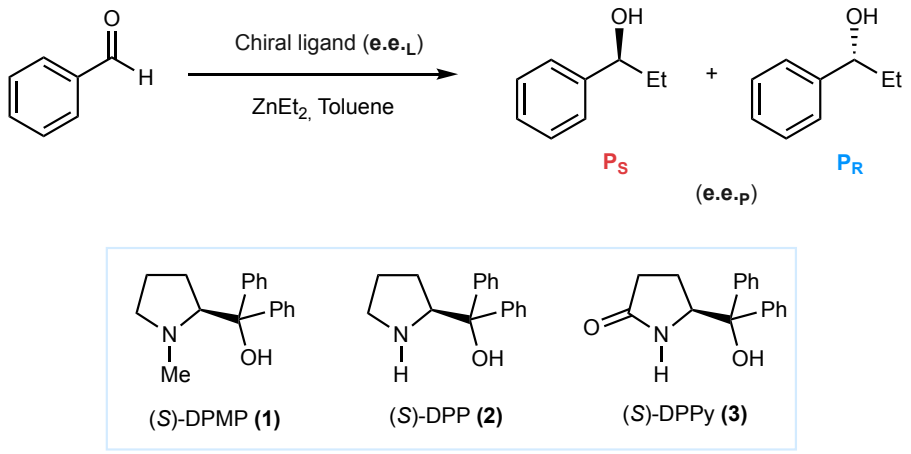

Figure 2. Enantioselective addition of dialkylzinc to benzaldehyde catalyzed by three chiral diphenylprolinol derivatives. Diphenyl-N-methyl-prolinol (**DPMP, 1**), diphenylprolinol (**DPP, 2**) and 5-(hydroxydiphenylmethyl)-2-pyrrolidinone (**DPPy, 3**).

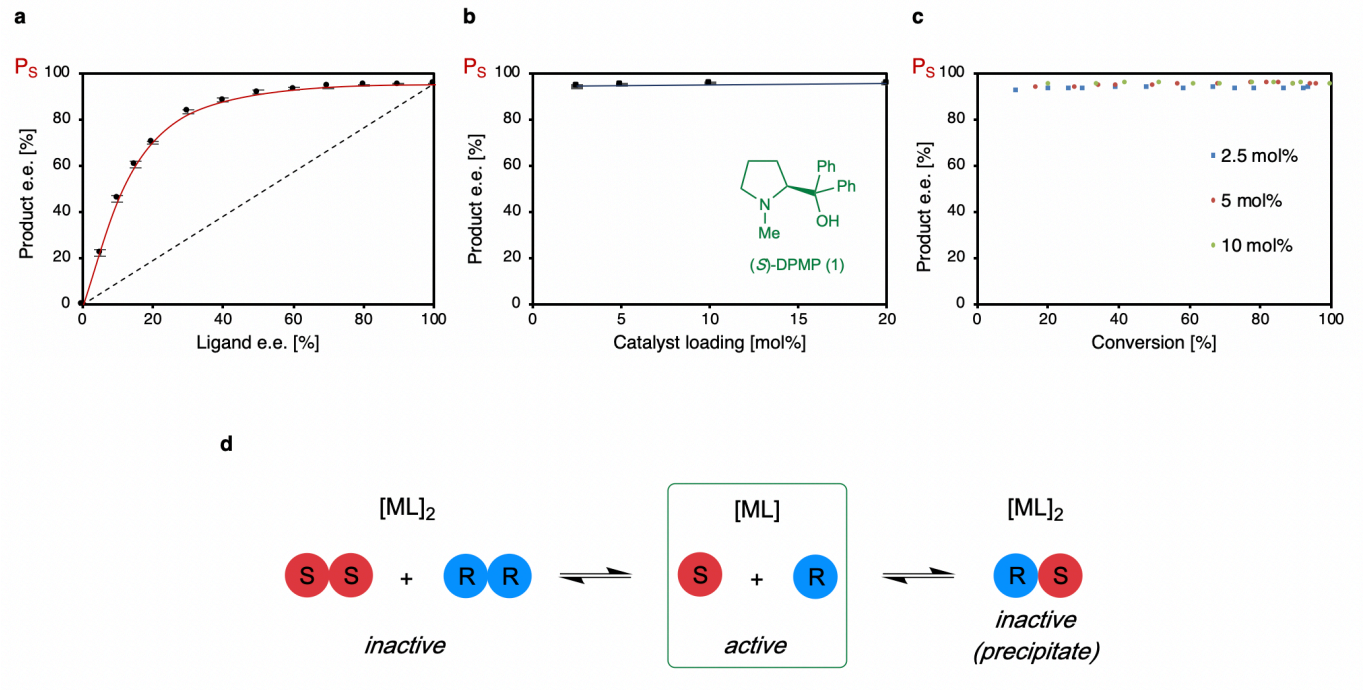

Figure 3. DPMP-catalysed addition of $ZnEt_2$ to benzaldehyde (0.15 M) at 20 °C in toluene as solvent. a) non-linear probing with 20 mol% of **1**; b) product ee as a function of catalyst loading using enantiopure **1**; c) product ee as a function of the conversion using enantiopure **1** at 2.5, 5 and 10 mol% catalyst loading. Positive values refer to the *(S)*-product in all cases. The reaction conditions and experimental procedure are described in the ESI. Each point is the mean of three different experiments, except in panel c; the vertical error bars depict standard deviations. The dashed line represents the linearity; the full line is a free-hand drawing, which serves as a guideline. D) Proposed model (each circle represents a mononuclear species of type [ML], M being the metal and L the ligand of R or S configuration).

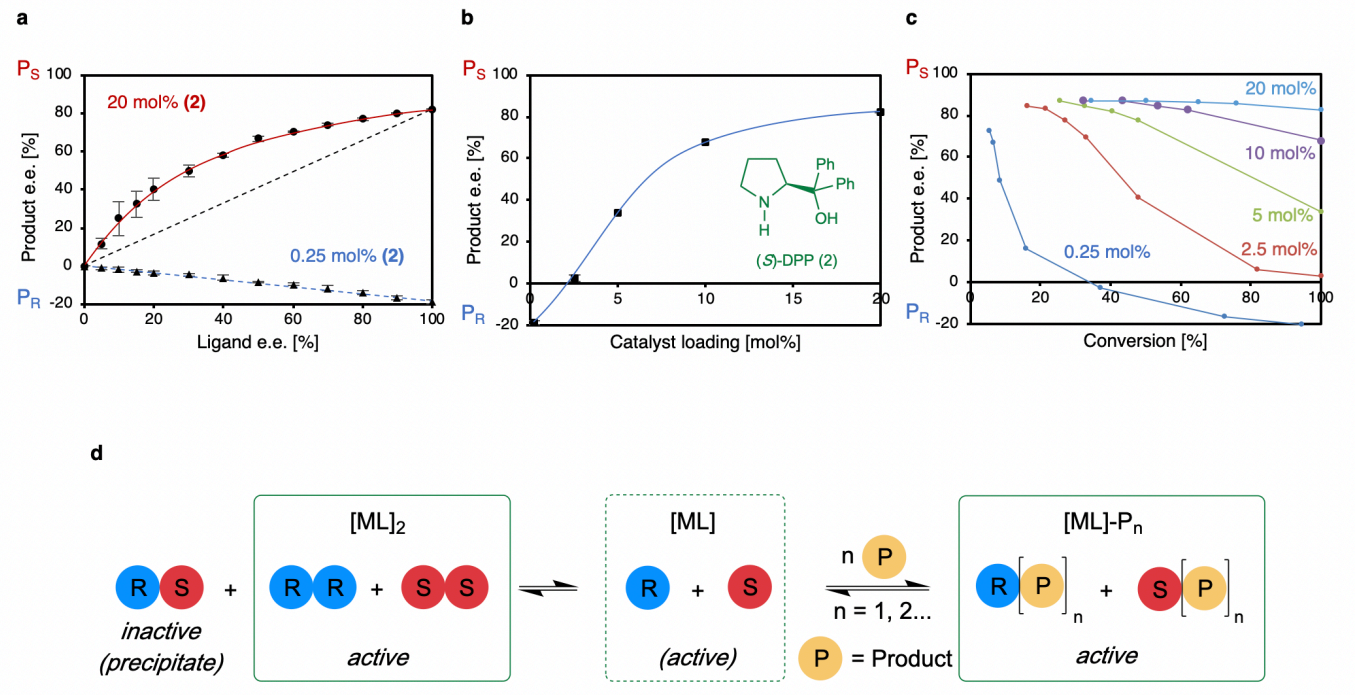

Figure 4. DPP (**2**)-catalysed addition of $ZnEt_2$ to benzaldehyde (0.4 M) at 20 °C in toluene as solvent. a) non-linear effect probing with 20 mol% (dots/red line) and 0.25 mol% (triangles/ blue line) of **2**; b) product ee as a function of catalyst loading using enantiopure **2**; c) product ee as a function of conversion at different catalyst loadings using enantiopure **2**. Positive ee_P values refer to the *S*-product in all cases. The reaction conditions and experimental procedure are described in the SI. Each point is the mean of three different experiments, except in panel c; the error bars depict standard deviations. The dashed lines simulate linear relationships; the full lines are free-hand drawings (a+b) or simple point-to-point lines (c), which serve as guidelines. d) Proposed catalytic system based on asymmetric induction. Dimeric homochiral [**2**-ZnEt]$_2$, monomeric **2**-ZnEt (to a limited extend, cf. discussion and Suppl. Fig. 12) and a **2**-ZnEt/product adduct (the stoichiometry of both components is unknown) are catalytically active and yield chiral product with opposite signs; the *meso* dimer precipitates. For the sake of clarity, the chirality of the product (and resulting catalyst/product diastereoisomers thereof) is omitted.

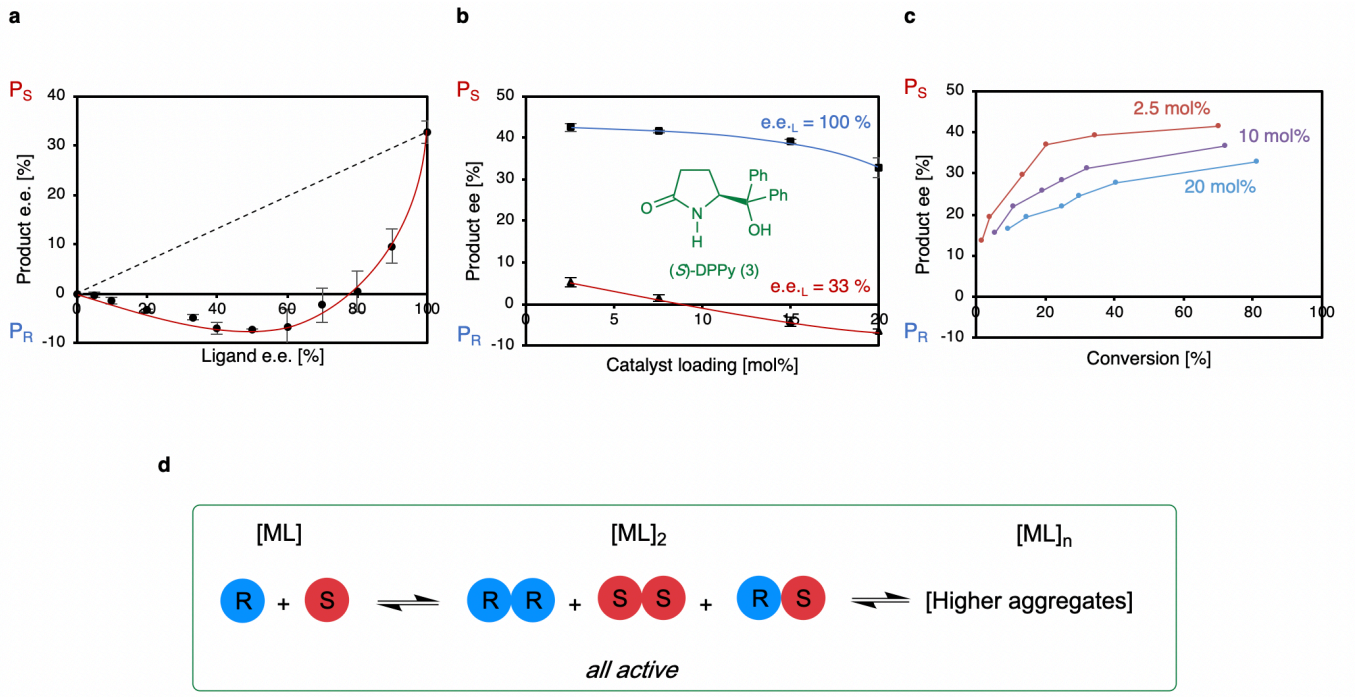

Figure 5. DPPy (**3**)-catalysed addition of $ZnEt_2$ to benzaldehyde (0.25 M) at 20 °C in toluene as solvent. a) non-linear effect probing with 20 mol% **3**; b) product ee as a function of catalyst loading using enantiopure **3** (dots/blue full line) and 33% ee_L **3** (triangles/red dotted line); c) product ee as a function of conversion at different catalyst loadings using enantiopure **3**. Positive ee_P values refer to the *S*-product in all cases. The reaction conditions and experimental procedure are described in the SI. Each point is the mean of three different experiments, except in panel c; the vertical error bars depict standard deviations. The dashed line simulates a linear relationship; the full lines are free-hand drawings, which serve as a guideline. d) Proposed model: monomeric **3**-ZnEt complexes aggregate to dimers and higher aggregates, of which possibly all are active – at least monomers or dimers and another, higher aggregation level.

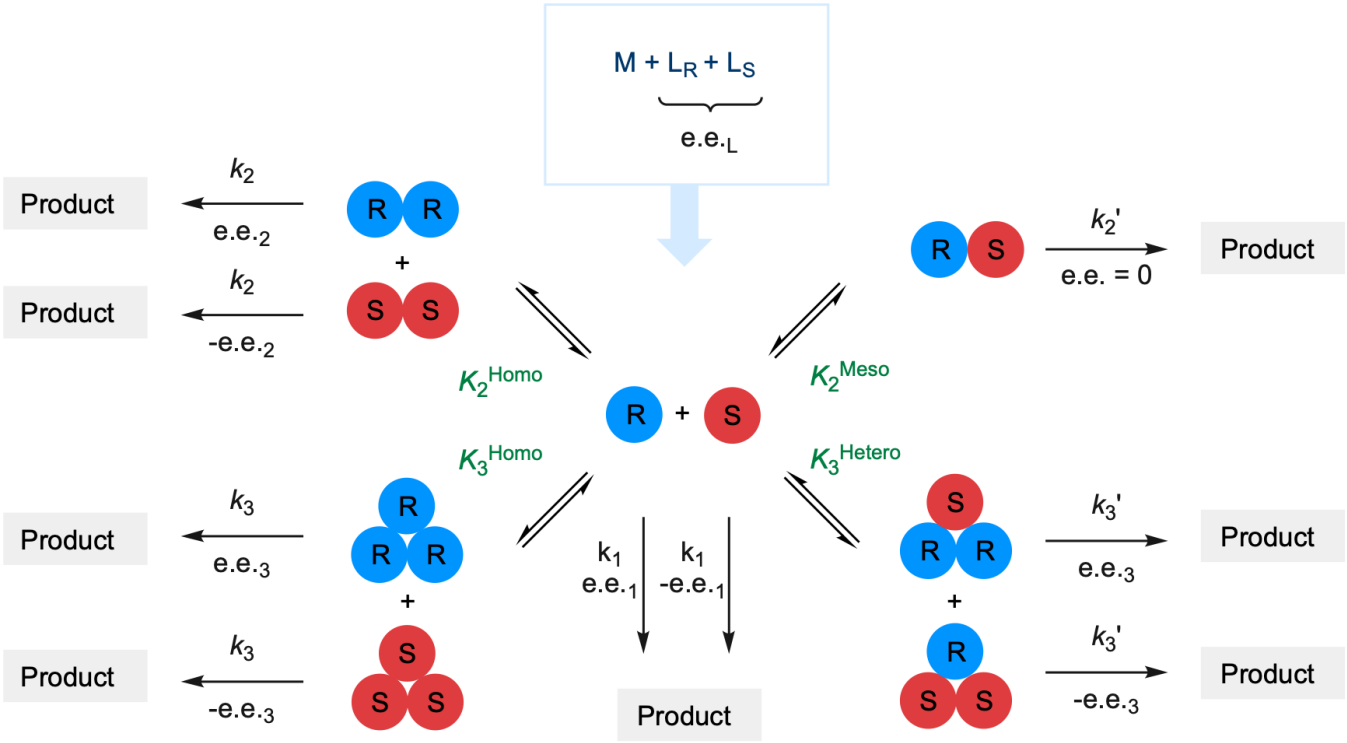

Figure 6. Developed scheme of the monomer-dimer-trimer competition model. Each species catalyses the reaction with a kinetic constant k and an enantioselectivity ee. Aggregates are defined as dimers or trimers of the monomers, related through the respective equilibrium constant K. In a pure dimer-trimer system the constants K are based on the homochiral dimers instead (cf. SI section III.2). The amount and composition of the different species is delimited by the overall ligand's ee (ee_L) and the total catalyst (or ligand) concentration [Cat_{tot}].

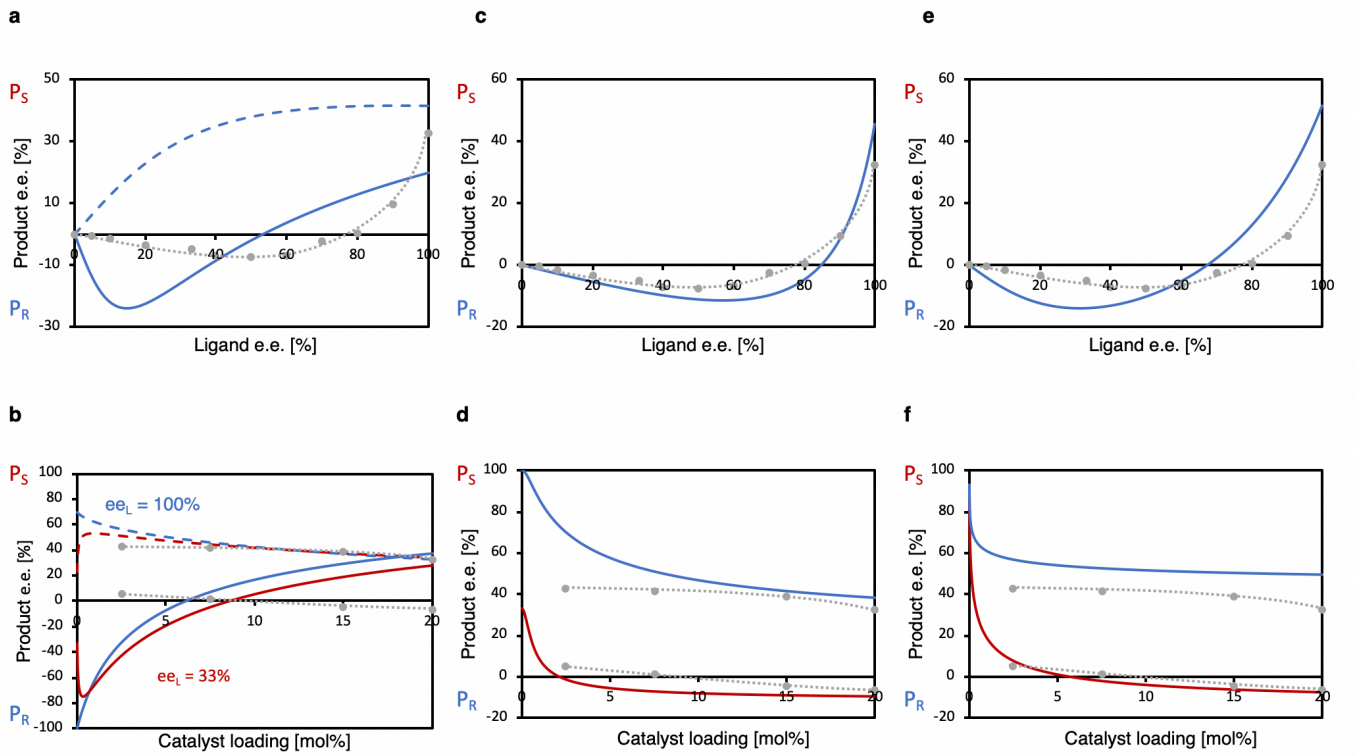

Figure 7. Simulations of NLE (top) and ee_P vs. cat. loading curves (bottom) in order to reproduce the main features of the data in Figure 4. a) + b): simulation accounting for monomeric and dimeric catalysts (ML1-2), plain lines k_1 = 10, k_2 = 1, k_2' = 0, K_2^{Homo} = 100. K_2^{Meso} = 1000, ee_1 = 70%, ee_2 = -100%, K_3^{Homo} = K_3^{Hetero} = 0; dashed lines k_1 = 1, k_2 = 3, k_2' = 0, K_2^{Homo} = 10. K_2^{Meso} = 1000, ee_1 = 100%, ee_2 = -100%, K_3^{Homo} = K_3^{hetero} = 0. c) + d): simulation accounting for monomeric and trimeric catalysts (ML1-3), k_1 = 20, k_3 = 33, k_3' = 250, K_3^{Homo} = 3000, K_3^{Hetero} = 10000, ee_1 = 100%, ee_3 = 20%, ee_3' = -40%, K_2^{Homo} = K_2^{Meso} = 0. e) + f): simulation accounting for dimeric and trimeric catalysts (ML2-3), k_2 = 100, k_2' = 0, k_3 = 33, k_3' = 250, K_2 = 100, $K_{2->3}^{Homo}$ = 250, $K_{2->3}^{Hetero}$ = 1000, ee_2 = 100%, ee_3 = 40%, ee_3' = -40%. All blue lines in b), d) and f) comprise ee_L = 100%, for red lines ee_L = 33%. Panels a), c) and e) all comprise [Cat_{tot}] = 0.1. For comparison, the NLE and ee_P vs catalyst loading data from Figure 4 is reproduced as grey dots/dotted lines.

References

1. Yoon, T. P. & Jacobsen, E. N. Privileged Chiral Catalysts. *Science* **299**, 1691–1693 (2003).
2. *Comprehensive Asymmetric Catalysis I - III*. (Springer Berlin, 1999).
3. *Catalytic Asymmetric Synthesis*. (Wiley, 2010).
4. Ma, L., Abney, C. & Lin, W. Enantioselective catalysis with homochiral metal–organic frameworks. *Chem. Soc. Rev.* **38**, 1248–1256 (2009).
5. Huang, S., Yu, H. & Li, Q. Supramolecular Chirality Transfer toward Chiral Aggregation: Asymmetric Hierarchical Self-Assembly. *Adv. Sci.* **8**, 2002132 (2021).
6. Puchot, C. *et al.* Nonlinear effects in asymmetric synthesis. Examples in asymmetric oxidations and aldolization reactions. *J. Am. Chem. Soc.* **108**, 2353–2357 (1986).
7. Guillaneux, D., Zhao, S.-H., Samuel, O., Rainford, D. & Kagan, H. B. Nonlinear effects in asymmetric catalysis. *J. Am. Chem. Soc.* **116**, 9430–9439 (1994).
8. Girard, C. & Kagan, H. B. Nonlinear Effects in Asymmetric Synthesis and Stereoselective Reactions: Ten Years of Investigation. *Angew. Chem. Int. Ed.* **37**, 2922–2959 (1998).
9. Satyanarayana, T., Abraham, S. & Kagan, H. B. Nonlinear Effects in Asymmetric Catalysis. *Angew. Chem. Int. Ed.* **48**, 456–494 (2009).
10. Klussmann, M. *et al.* Thermodynamic control of asymmetric amplification in amino acid catalysis. *Nature* **441**, 621 (2006).
11. Kalek, M. & Fu, G. C. Caution in the Use of Nonlinear Effects as a Mechanistic Tool for Catalytic Enantioconvergent Reactions: Intrinsic Negative Nonlinear Effects in the Absence of Higher-Order Species. *J. Am. Chem. Soc.* **139**, 4225–4229 (2017).
12. Ali, C., Blackmond, D. G. & Burés, J. Kinetic Rationalization of Nonlinear Effects in Asymmetric Catalytic Cascade Reactions under Curtin–Hammett Conditions. *ACS Catal.* 5776–5785 (2022) doi:10.1021/acscatal.2c00783.
13. Geiger, Y., Achard, T., Maisse-François, A. & Bellemin-Laponnaz, S. Hyperpositive nonlinear effects in asymmetric catalysis. *Nat. Catal.* **3**, 422–426 (2020).

14. Geiger, Y., Achard, T., Maisse-François, A. & Bellemin-Laponnaz, S. Observation of hyperpositive non-linear effect in catalytic asymmetric organozinc additions to aldehydes. *Chirality* **32**, 1250–1256 (2020).
15. Geiger, Y., Achard, T., Maisse-François, A. & Bellemin-Laponnaz, S. Hyperpositive non-linear effects: enantiodivergence and modelling. *Chem. Sci.* **11**, 12453–12463 (2020).
16. Geiger, Y., Achard, T., Maisse-François, A. & Bellemin-Laponnaz, S. Absence of Non-Linear Effects Despite Evidence for Catalyst Aggregation. *Eur. J. Org. Chem.* **2021**, 2916–2922 (2021).
17. Thierry, T., Geiger, Y. & Bellemin-Laponnaz, S. Observation of Hyperpositive Non-Linear Effect in Asymmetric Organozinc Alkylation in Presence of N-Pyrrolidinyl Norephedrine. *Molecules* **27**, 3780 (2022).
18. *Privileged Chiral Ligands and Catalysts*. (John Wiley & Sons, Ltd, 2011).
19. Kitamura, M., Okada, S., Suga, S. & Noyori, R. Enantioselective addition of dialkylzincs to aldehydes promoted by chiral amino alcohols. Mechanism and nonlinear effect. *J. Am. Chem. Soc.* **111**, 4028–4036 (1989).
20. Kitamura, M., Suga, S., Oka, H. & Noyori, R. Quantitative Analysis of the Chiral Amplification in the Amino Alcohol-Promoted Asymmetric Alkylation of Aldehydes with Dialkylzincs. *J. Am. Chem. Soc.* **120**, 9800–9809 (1998).
21. Pu, L. & Yu, H.-B. Catalytic Asymmetric Organozinc Additions to Carbonyl Compounds. *Chem. Rev.* **101**, 757–824 (2001).
22. Noyori, R. *Asymmetric Catalysis in Organic Synthesis*. (John Wiley, 1994).
23. Soai, K., Ookawa, A., Ogawa, K. & Kaba, T. Complementary catalytic asymmetric induction in the enantioselective addition of diethylzinc to aldehydes. *J. Chem. Soc., Chem. Commun.* 467 (1987) doi:10.1039/c39870000467.
24. Soai, K., Ookawa, A., Kaba, T. & Ogawa, K. Catalytic asymmetric induction. Highly enantioselective addition of dialkylzincs to aldehydes using chiral pyrrolidinylmethanols and their metal salts. *J. Am. Chem. Soc.* **109**, 7111–7115 (1987).
25. Geiger, Y. & Bellemin-Laponnaz, S. Non-Linear Effects in Asymmetric Catalysis: Impact of Catalyst Precipitation. *ChemCatChem* **14**, e202200165 (2022).
26. Burés, J. A Simple Graphical Method to Determine the Order in Catalyst. *Angew. Chem. Int. Ed.* **55**, 2028–2031 (2016).

27. Burés, J. Variable Time Normalization Analysis: General Graphical Elucidation of Reaction Orders from Concentration Profiles. *Angew. Chem. Int. Ed.* **55**, 16084–16087 (2016).
28. Nielsen, C. D.-T. & Burés, J. Visual kinetic analysis. *Chem. Sci.* **10**, 348–353 (2019).
29. Gesslbauer, S., Hutchinson, G., White, A. J. P., Burés, J. & Romain, C. Chirality-Induced Catalyst Aggregation: Insights into Catalyst Speciation and Activity Using Chiral Aluminum Catalysts in Cyclic Ester Ring-Opening Polymerization. *ACS Catal.* **11**, 4084–4093 (2021).
30. Alamillo-Ferrer, C., Hutchinson, G. & Burés, J. Mechanistic interpretation of orders in catalyst greater than one. *Nat. Rev. Chem.* **7**, 26–34 (2023).
31. Nakano, K., Nozaki, K. & Hiyama, T. Asymmetric Alternating Copolymerization of Cyclohexene Oxide and CO2 with Dimeric Zinc Complexes. *J. Am. Chem. Soc.* **125**, 5501–5510 (2003).
32. Nakano, K., Hiyama, T. & Nozaki, K. Asymmetric amplification in asymmetric alternating copolymerization of cyclohexene oxide and carbon dioxide. *Chem. Commun.* 1871–1873 (2005) doi:10.1039/B417973K.
33. Dreisbach, C., Wischnewski, G., Kragl, U. & Wandrey, C. Changes of enantioselectivity with the substrate ratio for the addition of diethylzinc to aldehydes using a catalyst coupled to a soluble polymer. *J. Chem. Soc., Perkin Trans. 1* 875–878 (1995) doi:10.1039/P19950000875.
34. Trost, B. M., Fettes, A. & Shireman, B. T. Direct Catalytic Asymmetric Aldol Additions of Methyl Ynones. Spontaneous Reversal in the Sense of Enantioinduction. *J. Am. Chem. Soc.* **126**, 2660–2661 (2004).
35. Bryliakov, K. P. Dynamic Nonlinear Effects in Asymmetric Catalysis. *ACS Catal.* **9**, 5418–5438 (2019).
36. The review by Bryliakov mentions also a zinc-catalysed step in the synthesis of efavirenz, but a more recent study concludes on other pathways than autoinduction, cf. Griffiths, G. J., Warm, A. Proposed Mechanism for the Enantioselective Alkynylation of an Aryl Trifluoromethyl Ketone, the Key Step in the Synthesis of Efavirenz. *Org. Process Res. Dev.* **20**, 803–813 (2016).
37. For interesting examples of designed asymmetric autoinduction, including reversal of enantioselectivity, see: Mayer, L. C., Heitsch, S., Trapp, O. Nonlinear Effects in Asymmetric Catalysis by Design: Concept, Synthesis, and Applications *Acc. Chem. Res.***55**, 3345-3361 (2022).

38. Trapp, O. Self-amplification of Enantioselectivity in Asymmetric Catalysis by Supramolecular Recognition and Stereodynamics. in *Supramolecular Catalysis* 55–67 (John Wiley & Sons, Ltd, 2022). doi:10.1002/9783527832033.ch4.
39. Storch, G. & Trapp, O. By-design enantioselective self-amplification based on non-covalent product–catalyst interactions. *Nature Chem* **9**, 179–187 (2017).
40. Scholtes, J. F. & Trapp, O. Design and synthesis of a stereodynamic catalyst with reversal of selectivity by enantioselective self-inhibition. *Chirality* **31**, 1028–1042 (2019).
41. Menke, J.-M. & Trapp, O. Controlling the Enantioselectivity in an Adaptable Ligand by Biomimetic Intramolecular Interlocking. *J. Org. Chem.* **87**, 11165–11171 (2022).
42. Soai, K., Ookawa, A., Kaba, T. & Ogawa, K. Catalytic asymmetric induction. Highly enantioselective addition of dialkylzincs to aldehydes using chiral pyrrolidinylmethanols and their metal salts. *J. Am. Chem. Soc.* **109**, 7111–7115 (1987).
43. Torres, M., Maisse-François, A. & Bellemin-Laponnaz, S. Highly Recyclable Self-Supported Chiral Catalysts for the Enantioselective α-Hydrazination of β-Ketoesters. *ChemCatChem* **5**, 3078–3085 (2013).
44. Bissessar, D., Achard, T. & Bellemin-Laponnaz, S. Robust and Recyclable Self-Supported Chiral Nickel Catalyst for the Enantioselective Michael Addition. *Adv. Synth. Catal.* **358**, 1982–1988 (2016).
45. Enthaler, S. Rise of the Zinc Age in Homogeneous Catalysis? *ACS Catal.* **3**, 150–158 (2013).
46. Athavale, S. V., Simon, A., Houk, K. N. & Denmark, S. E. Demystifying the asymmetry-amplifying, autocatalytic behaviour of the Soai reaction through structural, mechanistic and computational studies. *Nat. Chem.* **12**, 412–423 (2020).
47. Athavale, S. V., Simon, A., Houk, K. N. & Denmark, S. E. Structural Contributions to Autocatalysis and Asymmetric Amplification in the Soai Reaction. *J. Am. Chem. Soc.* **142**, 18387–18406 (2020).
48. Trapp, O. *et al.* In Situ Mass Spectrometric and Kinetic Investigations of Soai's Asymmetric Autocatalysis. *Chem. - Eur. J.* **26**, 15871–15880 (2020).
49. Trapp, O. Efficient Amplification in Soai's Asymmetric Autocatalysis by a Transient Stereodynamic Catalyst. *Front. Chem.* **8**, (2020).

50. Soai, K., Shibata, T., Morioka, H. & Choji, K. Asymmetric autocatalysis and amplification of enantiomeric excess of a chiral molecule. *Nature* **378**, 767–768 (1995).
51. Soai, K., Kawasaki, T. & Matsumoto, A. Asymmetric autocatalysis of pyrimidyl alkanol and related compounds. Self-replication, amplification of chirality and implication for the origin of biological enantioenriched chirality. *Tetrahedron* **74**, 1973–1990 (2018).
52. Geiger, Y. One Soai reaction, two mechanisms? *Chem. Soc. Rev.* **51**, 1206–1211 (2022).
53. Xiang, S.-H. & Tan, B. Advances in asymmetric organocatalysis over the last 10 years. *Nat. Commun.* **11**, 3786 (2020).
54. Han, B. *et al.* Asymmetric organocatalysis: an enabling technology for medicinal chemistry. *Chem. Soc. Rev.* **50**, 1522–1586 (2021).
55. Aukland, M. H. & List, B. Organocatalysis emerging as a technology. *Pure Appl. Chem.* **93**, 1371–1381 (2021).